Unprecedented Early Flux Excess in the Hybrid 02es-like Type Ia Supernova 2022ywc Indicates Interaction with Circumstellar Material

Shubham Srivastav[1] [ORCID], T. Moore[1] [ORCID], M. Nicholl[1] [ORCID], M. R. Magee[2] [ORCID], S. J. Smartt[3,1] [ORCID], M. D. Fulton[1] [ORCID], S. A. Sim[1] [ORCID],
J. M. Pollin[1] [ORCID], L. Galbany[4,5] [ORCID], C. Inserra[6] [ORCID], A. Kozyreva[7] [ORCID], Takashi J. Moriya[8,9] [ORCID], F. P. Callan[1] [ORCID], X. Sheng[1] [ORCID],
K. W. Smith[1] [ORCID], J. S. Sommer[10] [ORCID], J. P. Anderson[11,12] [ORCID], M. Deckers[13] [ORCID], M. Gromadzki[14] [ORCID], T. E. Müller-Bravo[4,5] [ORCID],
G. Pignata[15] [ORCID], A. Rest[16,17] [ORCID], and D. R. Young[1] [ORCID]

[1] Astrophysics Research Centre, School of Mathematics and Physics, Queen's University Belfast, Belfast BT7 1NN, UK; s.srivastav@qub.ac.uk
[2] Department of Physics, University of Warwick, Coventry, UK
[3] Department of Physics, University of Oxford, Denys Wilkinson Building, Keble Road, Oxford OX1 3RH, UK
[4] Institute of Space Sciences (ICE-CSIC), Campus UAB, Carrer de Can Magrans, s/n, E-08193 Barcelona, Spain
[5] Institut d'Estudis Espacials de Catalunya (IEEC), E-08034 Barcelona, Spain
[6] Cardiff Hub for Astrophysics Research and Technology, School of Physics & Astronomy, Cardiff University, Queens Buildings, The Parade, Cardiff, CF24 3AA, UK
[7] Heidelberger Institut für Theoretische Studien, Schloss-Wolfsbrunnenweg 35, D- 69118 Heidelberg, Germany
[8] National Astronomical Observatory of Japan, National Institutes of Natural Sciences, 2-21-1 Osawa, Mitaka, Tokyo 181-8588, Japan
[9] School of Physics and Astronomy, Faculty of Science, Monash University, Clayton, Victoria 3800, Australia
[10] Universitäts-Sternwarte München, Fakultät für Physik, Ludwig-Maximilians Universität München, Scheinerstr. 1, D-81679 Munich, Germany
[11] European Southern Observatory, Alonso de Córdova 3107, Casilla 19, Santiago, Chile
[12] Millennium Institute of Astrophysics MAS, Nuncio Monsenor Sotero Sanz 100, Off. 104, Providencia, Santiago, Chile
[13] School of Physics, Trinity College Dublin, College Green, Dublin 2, Ireland
[14] Astronomical Observatory, University of Warsaw, Al. Ujazdowskie 4, 00-478, Warszawa, Poland
[15] Instituto de Alta Investigación, Universidad de Tarapacá, Casilla 7D, Arica, Chile
[16] Space Telescope Science Institute, 3700 San Martin Drive, Baltimore, MD 21218, USA
[17] Department of Physics and Astronomy, Johns Hopkins University, 3400 North Charles Street, Baltimore, MD 21218, USA

Abstract

We present optical photometric and spectroscopic observations of the 02es-like type Ia supernova (SN) 2022ywc. The transient occurred in the outskirts of an elliptical host galaxy and showed a striking double-peaked light curve with an early excess feature detected in the ATLAS orange and cyan bands. The early excess is remarkably luminous with an absolute magnitude ~ -19, comparable in luminosity to the subsequent radioactively driven second peak. The spectra resemble the hybrid 02es-like SN 2016jhr, which is considered to be a helium shell detonation candidate. We investigate different physical mechanisms that could power such a prominent early excess and rule out massive helium shell detonation, surface ^{56}Ni distribution, and ejecta–companion interaction. We conclude that SN ejecta interacting with circumstellar material (CSM) is the most viable scenario. Semianalytical modeling with MOSFiT indicates that SN ejecta interacting with $\sim 0.05\ M_\odot$ of CSM at a distance of $\sim 10^{14}$ cm can explain the extraordinary light curve. A double-degenerate scenario may explain the origin of the CSM, by tidally stripped material from either the secondary white dwarf or disk-originated matter launched along polar axes following the disruption and accretion of the secondary white dwarf. A nonspherical CSM configuration could suggest that a small fraction of 02es-like events viewed along a favorable line of sight may be expected to display a very conspicuous early excess like SN 2022ywc.

Unified Astronomy Thesaurus concepts: Supernovae (1668); Type Ia supernovae (1728)

Supporting material: data behind figure

1. Introduction

Although supernovae of type Ia (SNe Ia) are valuable as cosmic distance indicators, the nature of their progenitor(s) and explosion mechanism(s) involved are still debated (Livio & Mazzali 2018; Jha et al. 2019). Modern wide-field surveys have unearthed a perplexing diversity within thermonuclear transients, indicating that multiple progenitor systems and underlying explosion mechanisms are likely responsible (Liu et al. 2023b).

Early time observations within the first few hours and days from explosion are a sensitive probe for the progenitors and

explosion mechanisms of SNe Ia (Maeda et al. 2018). Aided by early discovery and rapid classification, statistical studies of nearby and well-sampled light curves have revealed that a "bump" or "early flux excess" is a characteristic feature in a significant fraction of SNe Ia, ~20% (Deckers et al. 2022; Magee et al. 2022). The properties of the early excess are diverse, displaying a range of luminosities, colors, and timescales. Different physical mechanisms have been invoked to account for this feature: ejecta–companion interaction within a single-degenerate (SD) scenario (Kasen 2010), radioactive material in the surface layers of SN ejecta (Piro & Morozova 2016; Jiang et al. 2018; Polin et al. 2019; Magee et al. 2020), and interaction with extended circumstellar material (CSM; Piro et al. 2021; Moriya et al. 2023), within either the SD paradigm or double-degenerate (DD) paradigm.

Although an early excess has been observed in a handful of spectroscopically "normal" SNe Ia like SN 2017cbv (Hosseinzadeh et al. 2017), SN 2018oh (Dimitriadis et al. 2019; Li et al. 2019; Shappee et al. 2019), and SN 2023bee (Hosseinzadeh et al. 2023; Wang et al. 2023), this feature certainly appears to be more prevalent among members of spectroscopically peculiar Ia subclasses. A broad, blue bump is seen in a high fraction ($44\% \pm 13\%$) of the shallow silicon subclass of 91T/99aa-like SNe Ia (Jiang et al. 2018; Deckers et al. 2022). A short-lived ($\lesssim$1-day timescale), pulse-like early excess has recently been discovered in the rare carbon-rich, overluminous subclass of 03fg-like SNe Ia that include SN 2020hvf (Jiang et al. 2021), SN 2021zny (Dimitriadis et al. 2023), and SN 2022ilv (Srivastav et al. 2023).

A pronounced excess in blue and ultraviolet (UV) bands that lasts for a few days has been seen in members of the rare subclass of 02es-like SNe Ia, such as iPTF14atg (Cao et al. 2015) and SN 2019yvq (Miller et al. 2020; Burke et al. 2021). SN 2002es (Ganeshalingam et al. 2012) is the prototype of the 02es-like subclass that is characterized by normal-width but subluminous light curves, typically displaying peak absolute magnitudes of up to $\sim$1.5 mag fainter than normal SNe Ia. Spectroscopically, 02es-like events show prominent Ti II features in their photospheric spectra akin to sub-luminous 91bg-like SNe Ia, with lower ejecta velocities on average relative to normal SNe Ia (White et al. 2015). Similar to 91bg-like SNe Ia, 02es-like events show a preference for remote locations within early-type host galaxies (Taubenberger 2017).

A subset of 02es-like events display the unusual combination of a high peak luminosity comparable to normal SNe Ia, coupled with Ti II features in optical spectra around the peak, a characteristic associated with cool photospheres of sub-luminous 91bg-like Ia, and have thus been dubbed as "hybrid" 02es-like Ia (Jiang et al. 2017). SN 2016jhr (Jiang et al. 2017) is a well-studied hybrid 02es-like object and showed an early excess that was relatively red. Two other examples in the literature include SN 2006bt (Foley et al. 2010) and SN 2007cq (Ganeshalingam et al. 2010; Silverman et al. 2012), although these two events lack early time photometric coverage to investigate any early excess.

In this paper, we present optical photometric and spectroscopic observations of SN 2022ywc, a hybrid 02es-like Ia that exhibits a very conspicuous early excess several magnitudes brighter than any previous known examples within different SN Ia subclasses.

2. Discovery and Follow-up

The Asteroid Terrestrial-impact Last Alert System (ATLAS) is an all-sky survey comprised of 4×50 cm Schmidt telescopes, each with a $\sim$30 square degree field of view (Tonry et al. 2018b). The survey is carried out primarily in two broad filters—cyan or c band (roughly equivalent to a composite $g + r$) and orange or o band (roughly equivalent to a composite $r + i$). A quad of 4×30 s exposures is obtained for each field of view on a given night, typically reaching 5σ depths of $\sim$19 − 19.5 mag. Difference imaging is performed using the ATLAS all-sky reference catalog (Refcat2; Tonry et al. 2018a). The data stream is processed through the ATLAS transient science server in order to enable real-time detection and characterization of astrophysical transients (Smith et al. 2020).

AT 2022ywc was discovered by ATLAS on 2022 October 28.13 UT or Modified Julian Date (MJD) 59880.13, at a magnitude of 18.24 ± 0.06 in the c band and registered to the Transient Name Server (TNS), designated internally as ATLAS22bkfp (Tonry et al. 2022). ATLAS continued to observe the field, and AT 2022ywc was subsequently identified as a transient of interest on the internal ATLAS transient science server (Smith et al. 2020) because of its unusual double-peaked light curve. The transient was classified by the Advanced Public ESO Spectroscopic Survey of Transient Objects or ePESSTO+ (Smartt et al. 2015) as a 91bg-like SN Ia (Ihanec et al. 2022) with a spectrum obtained on MJD 59899.29, $\sim$19 days following the initial discovery.

The final photometry for SN 2022ywc in the c and o bands was obtained using the publicly available ATLAS forced photometry server (Shingles et al. 2021). The individual flux measurements from each nightly quad were combined into a single measurement in order to improve signal to noise, and also to obtain deeper limits in case of nondetections (a factor of $\sqrt{4}$ improvement in signal to noise, or $\sim$0.8 mag). The stacked forced photometry reveals a 3σ detection at $m_o = 20.27 \pm 0.26$ on MJD 59878.02, $\sim$2 days prior to the TNS discovery epoch.

Following the spectroscopic classification of SN 2022ywc as a peculiar SN Ia, and given the unusual nature of the light curve, we obtained further spectroscopic follow-up within ePESSTO+ using the ESO Faint Object Spectrograph and Camera v.2 (Snodgrass et al. 2008) instrument on the 3.6 m New Technology Telescope (NTT). The spectra were obtained on 3 additional epochs with Gr#13 (3700–9300 Å) and the 1″ slit, on MJDs 59914.16, 59935.17 and 59957.07. The spectra were reduced and calibrated using the ePESSTO+ data reduction pipeline.[18]

3. Analysis

3.1. Host Galaxy, Redshift, and Distance

SN 2022ywc was discovered in the outskirts of the elliptical galaxy WISEA J032210.70-425303.9. The redshift of the host galaxy, obtained from the NASA Extragalactic Database, is $z = 0.061913 \pm 0.000103$ (Jones et al. 2009). Assuming $H_0 = 70$ km s^{-1} Mpc^{-1} and a flat Universe with $\Omega_M = 0.3$, the derived luminosity distance is 278 Mpc, or a distance modulus of 37.22 mag. The SN is offset by $\sim$15″ from the galaxy nucleus, corresponding to a projected radial separation of $\sim$21 kpc at this distance. The Milky Way (MW) extinction in the line of sight is $A_V = 0.04$ mag (Schlafly & Finkbeiner 2011). The host extinction is expected to be minimal, given the remote location of the SN within its early-type host. For the analysis that follows, we assume a distance modulus $\mu = 37.22$ mag with a standard systematic uncertainty of 0.15 mag, and a total line-of-sight extinction of $A_V = 0.04$ mag, with $R_V = 3.1$.

3.2. Light-curve Properties

The extinction-corrected absolute magnitude light curve of SN 2022ywc in the c and o bands is shown in Figure 1. The phase is relative to o-band maximum for SN 2022ywc on MJD 59896.0 ± 2.0. The epoch of maximum and the peak magnitude in o band was estimated using a third order polynomial fit to the points around the peak, excluding the early excess. The uncertainty on the o-band peak magnitude was estimated by adding the errors on the measurements around peak in quadrature. Also shown for comparison are the
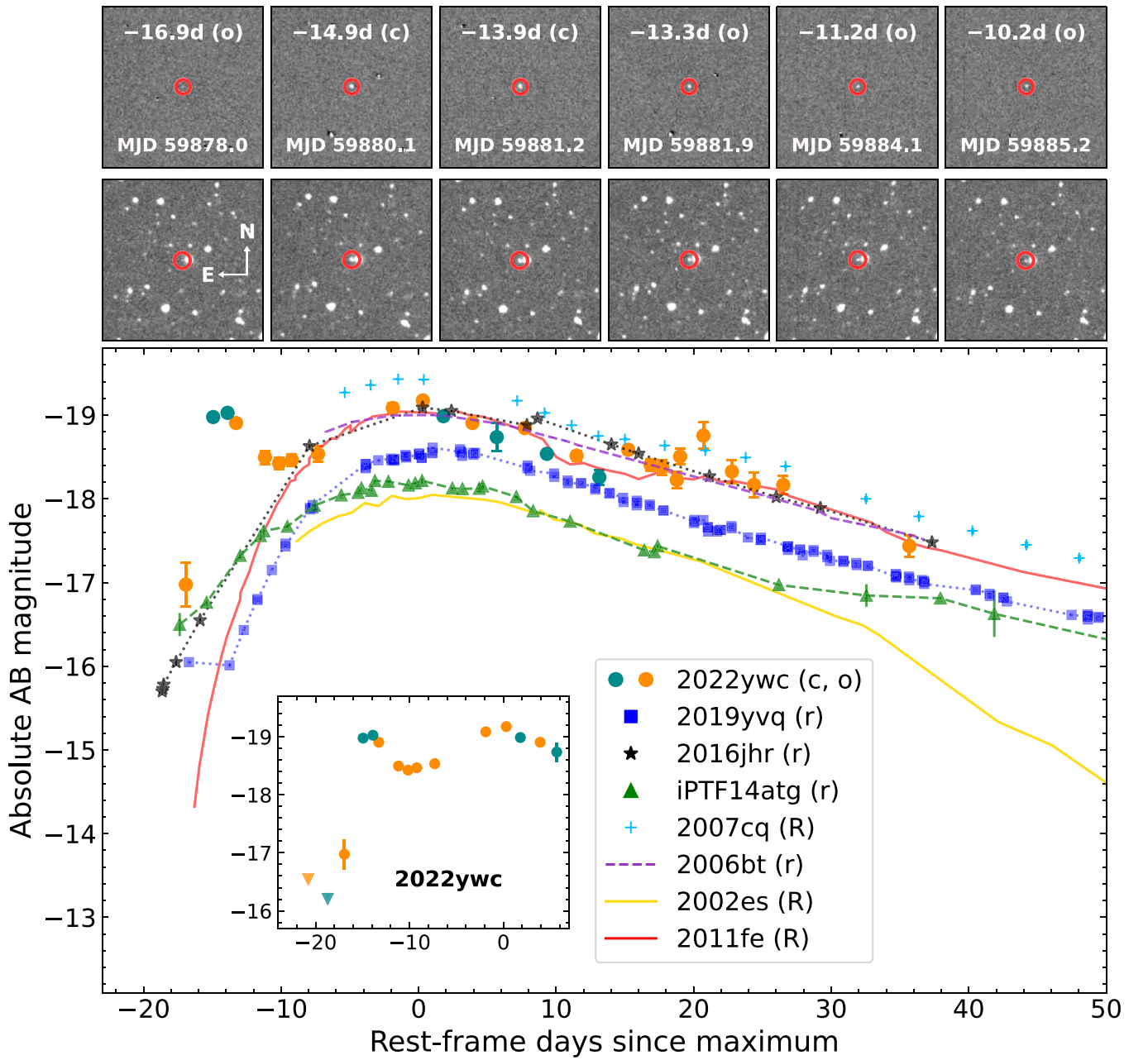
---

18 https://github.com/svalenti/pessto

Figure 1. Top and middle panels: Sequence of stacked difference and input images for SN 2022ywc during the early excess. The SN position is marked with a red circle. The image stamps cover a field of view of approximately $6' \times 6'$. Bottom panel: Absolute AB magnitude light curve of SN 2022ywc in the ATLAS c, o bands, corrected for MW extinction. Also shown for comparison are the MW extinction-corrected light curves of 02es-like events SN 2002es (Ganeshalingam et al. 2012), SN 2006bt (Foley et al. 2010), SN 2007cq (Ganeshalingam et al. 2010), iPTF14atg (Cao et al. 2015), SN 2016jhr (Jiang et al. 2017), and SN 2019yvq (Miller et al. 2020), and also the normal Ia SN 2011fe (Zhang et al. 2016). The inset highlights the strikingly luminous early excess for SN 2022ywc. The observed ATLAS photometry of SN 2022ywc shown in the lower panel of this figure is available as the data behind the figure.

(The data used to create this figure are available.)

absolute magnitude r/R-band light curves of other 02es-like events SN 2002es (Ganeshalingam et al. 2012), SN 2006bt (Foley et al. 2010), SN 2007cq (Ganeshalingam et al. 2010), iPTF14atg (Cao et al. 2015), SN 2016jhr (Jiang et al. 2017), and SN 2019yvq (Miller et al. 2020), along with the normal Ia SN 2011fe (Zhang et al. 2016). r/R band was chosen for a direct comparison since it is the closest to and overlaps with the two ATLAS filters. The literature objects were corrected only for MW extinction, since there is no discernible evidence for significant host extinction. Except for SN 2002es, SN 2006bt,

and SN 2007cq where early time photometric coverage is lacking, all the comparison Ia-02es events have a known early excess. The inset in Figure 1 shows the early time light curve of SN 2022ywc in more detail, highlighting the conspicuous early excess with no precedent in the literature.

As shown in Figure 1, 02es-like SNe Ia are typically subluminous with peak luminosity ∼1 mag fainter than that of normal SNe Ia. SN 2022ywc attains a peak luminosity of $M_o \approx -19.2 \pm 0.2$, however, comparable to normal SNe Ia. SN 2022ywc shares this characteristic with at least three other

02es-like events in the literature—SN 2006bt (Foley et al. 2010), SN 2007cq (Ganeshalingam et al. 2010), and SN 2016jhr (Jiang et al. 2017), together constituting the rare subclass of hybrid 02es-like Ia. Alongside the timescale and luminosity, the color of the early excess is also a useful diagnostic tool for investigating the physical origin of this feature. In the case of iPTF14atg (Cao et al. 2015) and SN 2019yvq (Miller et al. 2020; Burke et al. 2021), the excess was blue and quite pronounced in the near-UV bands, whereas it was relatively red in the case of SN 2016jhr (Jiang et al. 2017). The light curve of SN 2022ywc indicates the early excess was relatively blue, with $(c - o) \equiv (g - i) \lesssim 0$. However, since we only have photometry in the two ATLAS bands, and no concurrent early time spectroscopic observations, a robust assessment for the color of the excess feature is difficult to make.

3.3. Light-curve Fitting

It is evident that the double-peaked light curve of SN 2022ywc cannot be accounted for by a standard model powered by ^{56}Ni decay alone. The plausible mechanisms that could potentially explain the luminous early excess are ejecta–companion interaction (Kasen 2010), CSM interaction (Piro & Morozova 2016; Piro et al. 2021), helium (He) shell detonation (Polin et al. 2019; Magee et al. 2021), and surface ^{56}Ni distribution (Jiang et al. 2018; Magee et al. 2020). If one of the latter two scenarios were responsible, a very large amount of surface ^{56}Ni or an extremely thick He shell would be necessary, given the excess feature is comparable in luminosity to the second peak. Copious amounts of iron-group elements (IGEs) and intermediate mass elements (IMEs) in the outer ejecta would in turn induce severe line-blanketing at bluer wavelengths, although the spectra (Section 3.4) do not show evidence of the same. We discuss the viability and shortcomings of the competing scenarios in more detail in Section 4. In this Section, we focus on modeling the light curve of SN 2022ywc with a composite model combining ^{56}Ni decay and CSM interaction. We employ the publicly available Modular Open Source Fitter for Transients (MOSFiT; Nicholl et al. 2017; Guillochon et al. 2018). MOSFiT takes as input the multiband photometry of the transient and priors on the parameters for the model being fit to the data. MOSFiT has a built-in model CSMNI that combines the luminosity from the decay of radioactive ^{56}Ni and additional luminosity from CSM interaction, wherein a fraction of the kinetic energy of SN ejecta is converted to radiative energy through collision with dense CSM. The treatment of ^{56}Ni and ^{56}Co decay is from Nadyozhin (1994), while the physics of CSM interaction is based on the semianalytic treatment in Chatzopoulos et al. (2013).

The model is set up such that the contribution from CSM interaction begins at time $t \sim R_0/v_{ej}$, where R_0 is the inner radius of the CSM shell, and v_{ej} is the bulk velocity of SN ejecta. The model has 10 free parameters, namely total ejecta mass (M_{ej}), ^{56}Ni mass fraction ($f_{Ni} \equiv M_{Ni}/M_{ej}$), kinetic energy ($E_k$), mass of the CSM shell (M_{CSM}), inner radius of the CSM shell (R_0), CSM density at the initial radius R_0 (ρ_0), time of explosion relative to first epoch of observation (t_{exp}), minimum temperature (T_{min}), host galaxy extinction (A_V^{host}), and a white-noise variance term (σ). T_{min} represents the constant temperature that the expanding and cooling photosphere settles down to, and σ represents the additional uncertainty (in magnitudes) that would make the reduced $\chi^2 = 1$. A power-law density profile for the CSM shell is adopted with $\rho(r) = qr^{-s}$, where

the scaling factor $q = \rho_0 R_0^s$ (Chatzopoulos et al. 2012). The power-law index was fixed to $s = 2$ corresponding to a steady-wind CSM model (eg., Chevalier & Irwin 2011). The γ-ray opacity was fixed at $\kappa_\gamma = 0.027$ cm^2 g^{-1} (Cappellaro et al. 1997). An average photospheric velocity for the SN ejecta is inferred from the free parameters M_{ej} and E_k assuming a constant density (Arnett 1982), using

$$E_k \approx \frac{3}{10} M_{ej} v_{ej}^2. \tag{1}$$

We use the dynamic nested sampling approach within MOSFiT implemented using the DYNESTY package (Speagle 2020) to evaluate the posterior distributions of the model parameters. Broad priors were assigned for the free parameters, with $M_{ej} \in [0.1, 2.0] M_\odot$ to allow for a range of WD progenitor masses and $E_k \in [0.1, 2.0] \times 10^{51}$ erg, informed by constraints on the ejecta velocity from spectroscopic observations. Since we have a good constraint on the explosion epoch from high-cadence pre-discovery nondetections (Figure 2), a narrow prior of $t_{exp} \in [-4, 0]$ days was set, where t_{exp} is defined relative to the first photometric observation on MJD 59878.02. We use log-flat priors for parameters with a range that spans 2 or more orders of magnitude in order to allow for a more efficient and robust exploration of the parameter space.

Table 1 summarizes the priors and the best-fit median values and 1σ bounds for the free parameters in the CSMNI model for SN 2022ywc. The light-curve fit is shown in Figure 2, and Figure 3 shows a corner plot with 2D posteriors for the model parameters.

The CSMNI model reproduces the timescale, luminosity, and color of the early excess and also the second peak and overall light-curve shape fairly well. The most interesting physical parameters in the model are the explosion parameters M_{ej}, M_{Ni}, and E_k, and the key CSM parameters M_{CSM} and R_0. The key parameters are well-constrained, as seen in Figure 3. $M_{ej} = 1.24^{+0.15}_{-0.13} M_\odot$ is consistent with either a near Chandrasekhar-mass (M_{Ch}) or M_{Ch} WD progenitor within the uncertainties. The ^{56}Ni fraction f_{Ni} implies $M_{Ni} = 0.73^{+0.21}_{-0.17} M_\odot$, compatible with normal SN Ia luminosity. An average ejecta velocity, inferred from the median M_{ej} and E_k from the fit, is $v_{ej} \sim 13,000$ km s^{-1}. This is comparable to the Si II $\lambda 6355$ velocity measured for SN 2022ywc (Section 3.4), and consistent with the photospheric velocity of hybrid 02es-like Ia SN 2006bt (Foley et al. 2010) and SN 2016jhr (Jiang et al. 2017) around the peak. The model requires $\sim 0.05 M_\odot$ of CSM at $\sim 3 \times 10^{14}$ cm from the WD progenitor in order to explain the early excess. We note here that the Chatzopoulos et al. (2013) model assumes optically thick interaction and may therefore be unreliable at low CSM masses. The model favors a minimal host extinction as expected, and the estimated time of explosion is MJD $59875.1^{+0.6}_{-0.7}$.

3.4. Spectroscopic Properties

The four NTT spectra obtained for SN 2022ywc at rest-frame phases +3d, +17d, +37d, and +58d relative to the time of maximum (MJD 59896.0) are shown in Figure 4. Also shown for comparison are spectra of the hybrid 02es-like events SN 2016jhr (Jiang et al. 2017), SN 2007cq (Ganeshalingam et al. 2010), and SN 2006bt (Foley et al. 2010; Silverman et al. 2012), the 91bg-like SN 1999by (Matheson et al. 2008), and also the normal Ia SN 2011fe (Mazzali et al. 2014; Zhang et al. 2016). The spectra were
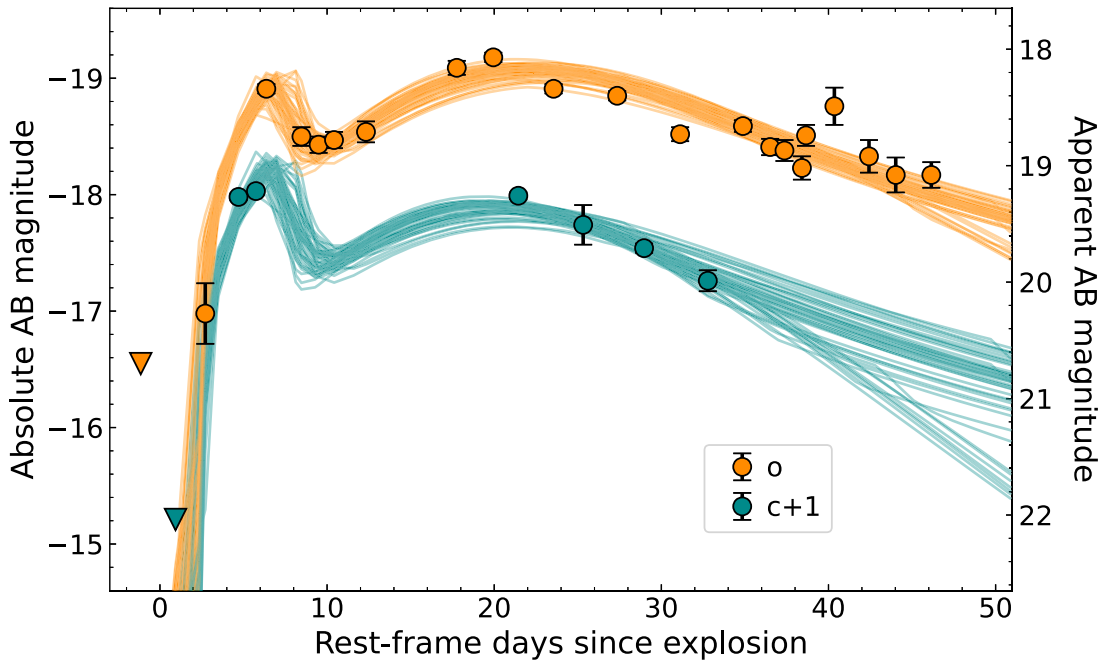
Figure 2. ATLAS light curve of SN 2022ywc along with draws from the posterior of the CSMNI model from MOSFiT. The *c*-band light curve and model are shifted for clarity. The explosion epoch, which is one of the free parameters in the model, is MJD $59875.1^{+0.6}_{-0.7}$.

Table 1
Summary of Priors and Median Values with 16th/84th Percentiles of the
Marginalized Posteriors for the CSMNI Model Parameters

Parameter	Units	Prior	Prior Type	Best Fit
M_{ej}	$M_\odot$	[0.1, 2]	flat	$1.24^{+0.15}_{-0.13}$
f_{Ni}	dimensionless	[0.01, 1]	log-flat	$0.59^{+0.09}_{-0.08}$
E_k	10^{51} erg	[0.1, 2]	flat	$1.28^{+0.32}_{-0.28}$
M_{CSM}	$M_\odot$	[0.001, 1]	log-flat	$0.05^{+0.01}_{-0.01}$
R_0	10^{14} cm	[0.015, 15]	log-flat	$2.73^{+0.58}_{-0.84}$
ρ_0	10^{-13} g cm^{-3}	[0.01, 100]	log-flat	$1.55^{+2.17}_{-0.70}$
t_{exp}	days	[−4, 0]	flat	$-2.88^{+0.64}_{-0.67}$
T_{min}	10^3 K	[0.1, 100]	log-flat	$5.89^{+1.42}_{-1.36}$
A_V^{host}[a]	mag	[0.0, 5.6]	log-flat	$0.002^{+0.036}_{-0.002}$

Note.

[a] The free parameter in the model is the hydrogen column density along the line of sight within the host galaxy, N_H^{host}. We use a prior of $N_H^{host} \in [10^{16}, 10^{22}]$ cm^{-2}. The host extinction is computed from the column density using the relation $A_V^{host} \approx N_H^{host}/(1.8 \times 10^{21})$ mag (Predehl & Schmitt 1995).

corrected for MW extinction (Schlafly & Finkbeiner 2011) and Doppler-corrected to the rest frame. The first spectrum for SN 2022ywc at +3d exhibits a fairly blue continuum similar to the comparison SNe, and in contrast to the likes of massive He shell detonation candidates SN 2020jgb (Liu et al. 2023a), SN 2018byg (De et al. 2019), and SN 2016dsg (Dong et al. 2022), that shows a red continuum blue-ward of ∼5000 Å in spectra around peak due to substantial line-blanketing from IMEs and IGEs synthesized within the He ash.

From the first spectrum of SN 2022ywc at +3d, we measure a Si II $\lambda6355$ velocity of ∼9800 ± 400 km s^{-1}. The "W" feature ∼5500 Å attributed to S II is noticeably weaker in SN 2022ywc when compared to SN 2016jhr, SN 2006bt, and SN 2011fe. The most conspicuous feature in the +3d spectrum of SN 2022ywc is the broad absorption blend ∼4500 Å, attributable to Ti II. The

presence of Ti II features in the spectra has been suggested as evidence for products of He shell burning in the double detonation scenario (eg., Kromer et al. 2010; Polin et al. 2019; Collins et al. 2022). 02es-like SNe Ia are often classified as 91bg-like owing to the presence of strong Ti II features around 4000–5000 Å. However, there are subtle differences, with 91bg-like Ia showing stronger O I and Ca II features. These differences, in conjunction with the distinct photometric behavior (i.e., slower decline rate and higher luminosity for 02es-like Ia), can be used to tell these subclasses apart.

The spectra of SN 2022ywc show a good overall match with the hybrid 02es-like SN 2006bt (Foley et al. 2010), SN 2007cq (Ganeshalingam et al. 2010), and SN 2016jhr (Jiang et al. 2017). The early spectra show marked differences with the normal Ia SN 2011fe, especially at bluer wavelengths. However, the later spectra at +37d and +58d are much closer to SN 2011fe. The +3d spectrum of SN 2022ywc does not show any obvious signatures of He although this does not necessarily rule out its presence in the ejecta, since formation of He lines requires nonthermal excitation (eg., Hachinger et al. 2012). Moreover, simulations show that He lines may be easier to detect at near-infrared wavelengths, specifically the He I $\lambda10830$ feature (Collins et al. 2023).

In Figure 4 (top panel), we compare the +3d spectrum of SN 2022ywc with synthetic spectra from the double detonation models of Polin et al. (2019) in order to place rough limits on the amount of He that could be present in the SN ejecta. We chose models with He shell masses of 0.01, 0.03, and 0.05 $M_\odot$. The Polin et al. (2019) models are computed at 0.25 day intervals. For comparison with SN 2022ywc, we computed the time of *r*-band maximum from the synthetic model light curves, and selected the epoch that is closest to the phase of +3d for the observed spectrum. The models with a WD mass of 1.0 $M_\odot$ were chosen for the comparison, since their predicted peak luminosity is closest to that observed for SN 2022ywc. The strength of the Ti II trough observed in SN 2022ywc is roughly consistent with the 0.03 $M_\odot$ He shell model. The models with
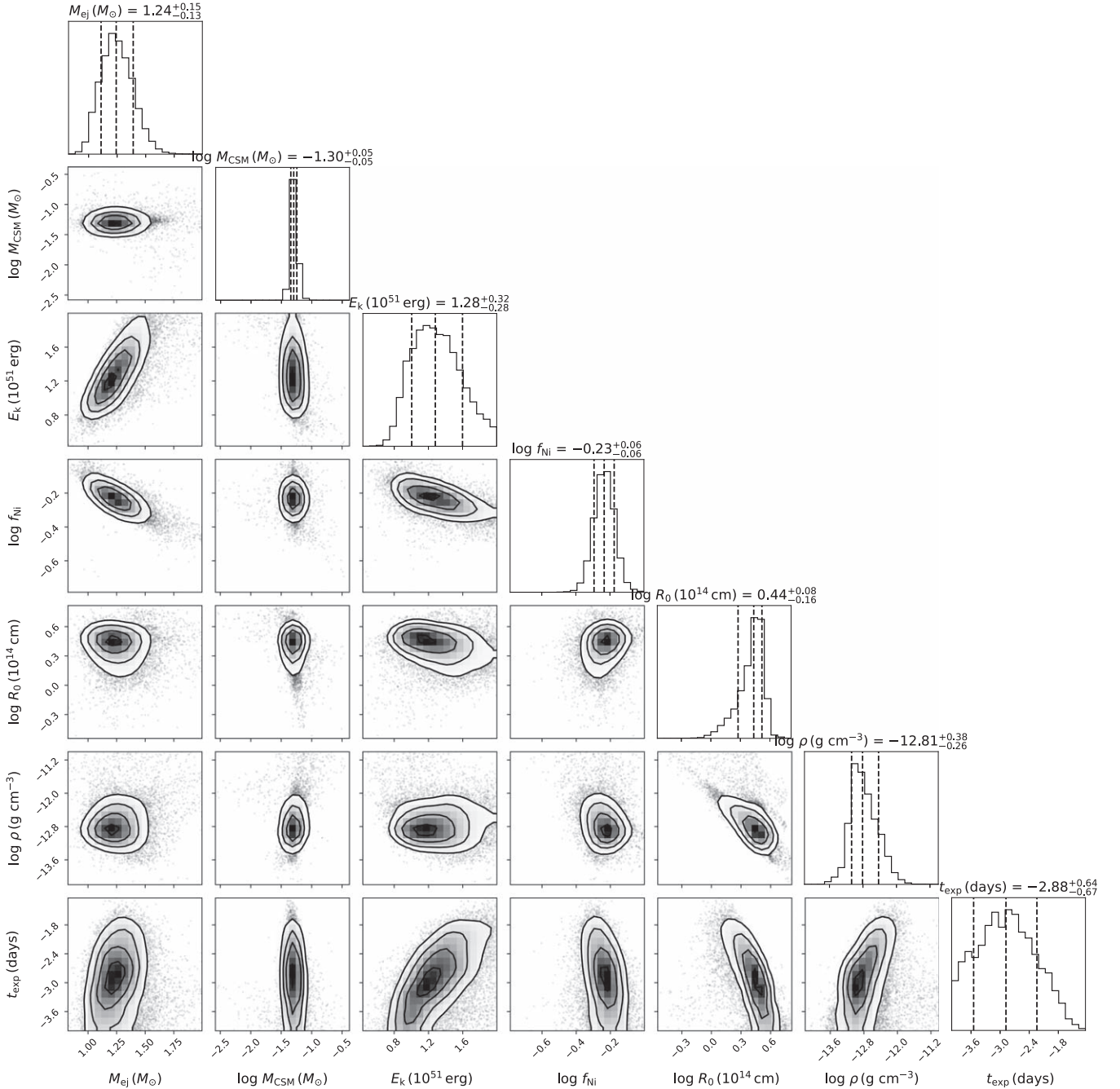
Figure 3. 2D posteriors for the main physical parameters in the `MOSFiT` CSMNI model fit to SN 2022ywc. R_0 is in units of 10^{14} cm, and t_{exp} is relative to MJD 59878.02.

He shell masses of 0.05 $M_\odot$ and higher are much redder than SN 2022ywc due to significant UV line-blanketing at bluer wavelengths. On the other hand, the models with higher WD masses of 1.1 and 1.2 $M_\odot$ are significantly brighter at bluer wavelengths, and show a poor match to the continuum shape of the observed +3d spectrum of SN 2022ywc.

We note that, for surface radioactivity scenarios such as ^{56}Ni mixing and He shell detonation, the specific composition of radioactive isotopes can significantly affect the observational signatures. Magee et al. (2021) explored the effects of different He shell compositions on the photometric and spectroscopic properties and found it can have a big impact. For example, the

models with a post-explosion He shell composition that is dominated by IMEs such as ^{32}S and ^{36}Ar are considerably bluer around the peak compared to models with shell composition dominated by IGEs such as ^{44}Ti, ^{48}Cr, ^{52}Fe, and ^{56}Ni (eg., Magee et al. 2021).

4. Discussion

4.1. Physical Scenarios for the Early Excess

An early flux excess in the light curve has been discovered in all 02es-like SNe Ia in recent times that have early time photometric coverage—iPTF14atg (Cao et al. 2015),
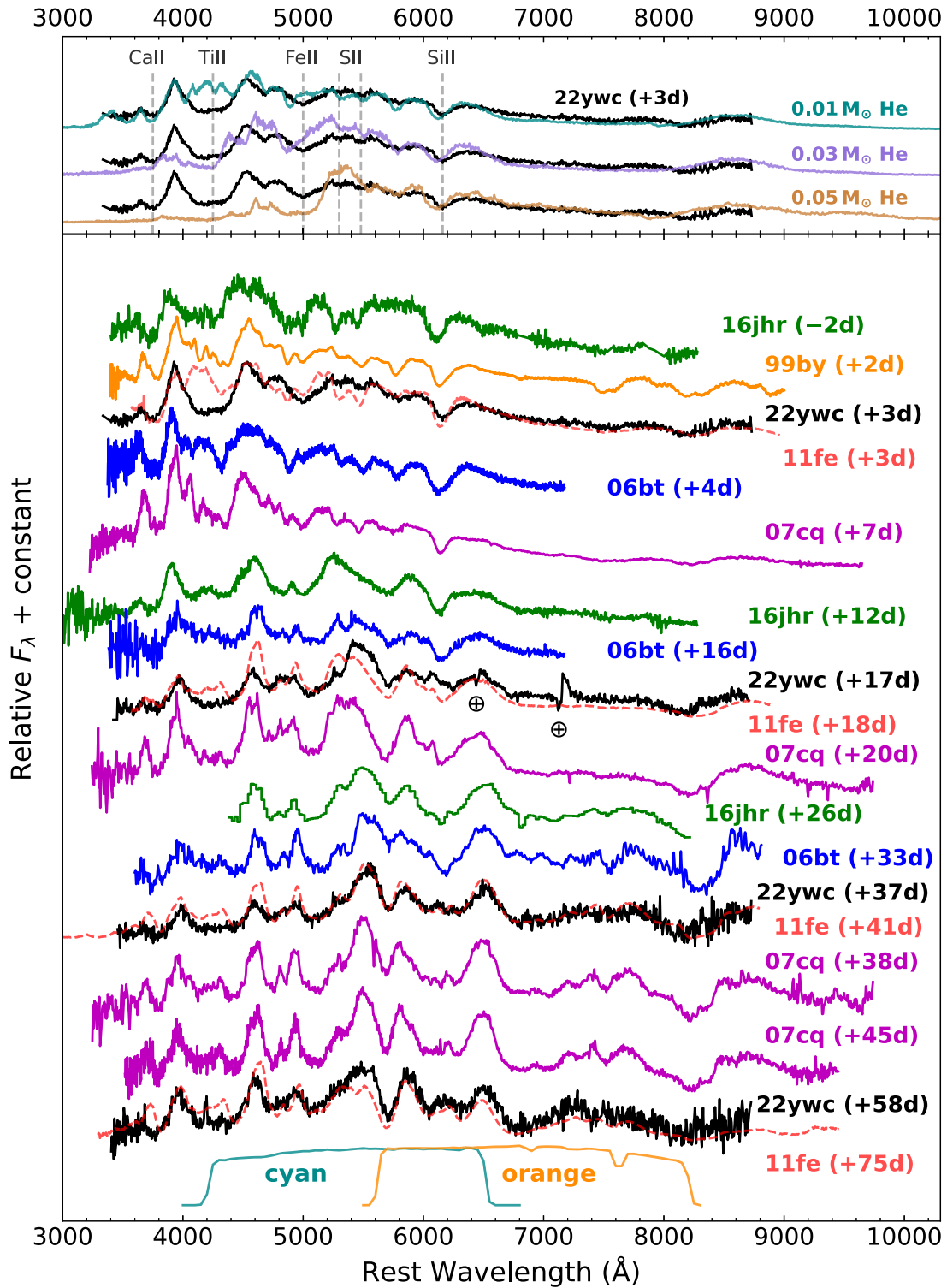
Figure 4. Spectral evolution of SN 2022ywc between +3d and +58d relative to maximum. Also plotted for comparison are the spectra of the hybrid 02es-like Ia SN 2006bt (Foley et al. 2010), SN 2007cq (Ganeshalingam et al. 2010), and SN 2016jhr (Jiang et al. 2017), the 91bg-like SN 1999by (Matheson et al. 2008) and the normal Ia SN 2011fe (Mazzali et al. 2014; Zhang et al. 2016) at similar phases. Top panel shows the +3d spectrum of SN 2022ywc compared to three double detonation models of Polin et al. (2019), computed for a WD mass of $1.0\,M_\odot$ and He shell masses of 0.01, 0.03, and $0.05\,M_\odot$. The model spectra were shifted along y-axis for clarity, but not scaled in wavelength or flux axes relative to the observed spectrum. Prominent telluric features are marked with the symbol $\oplus$. The ATLAS orange and cyan filter response curves are also shown for reference.

iPTF14dpk (Cao et al. 2016; Jiang et al. 2018; Burke et al. 2021), SN 2016jhr (Jiang et al. 2017), SN 2019yvq (Miller et al. 2020; Burke et al. 2021), and SN 2022ywc (this work). This is likely a generic feature of this subclass, thus serving as

an effective tool to investigate the progenitor scenario and explosion mechanism. In Section 3.3, we fit the early excess in the light curve of SN 2022ywc with a CSM interaction model using MOSFiT. The model yields a CSM mass of
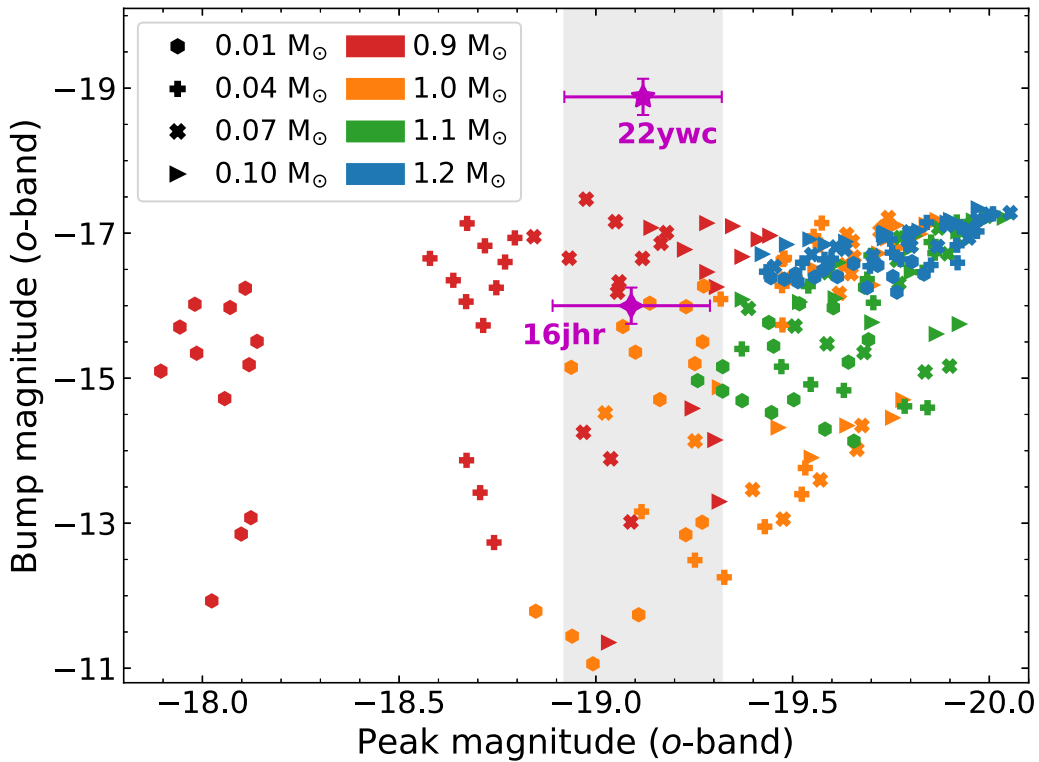
Figure 5. Predicted peak luminosity vs. luminosity for the bump or early excess in the double detonation models of Magee et al. (2021) computed for *o* band. The colors represent the WD masses, and symbols represent the He shell mass. The shaded region highlights the models with a peak luminosity that is consistent with that of SN 2022ywc. The peak magnitude of SN 2022ywc and the associated uncertainty were estimated using the method described in Section 3.2.

$M_{\rm CSM} \approx 0.05 M_{\odot}$, with an inner radius $R_0 \approx 3 \times 10^{14}$ cm (Table 1). We now consider alternative physical mechanisms that could plausibly explain the early excess instead.

At an absolute magnitude of ~ -19, the early excess for SN 2022ywc is comparable in luminosity to the main peak. Given we require a ^{56}Ni mass of $M_{\rm Ni} \approx 0.7 M_{\odot}$ for the main peak, a comparable and therefore very large amount of surface ^{56}Ni due to mixing or an extremely thick He shell would have to be invoked to explain the early excess in terms of surface radioactivity (Polin et al. 2019; Magee et al. 2020, 2021). The ATLAS $(c - o)$ color (Figure 2) and spectroscopic observations (Figure 4) do not show evidence of heavy line-blanketing effects at bluer wavelengths that would be expected from a large amount of radioactive material in the surface layers, thereby disfavoring these two scenarios. To illustrate this further, Figure 5 shows the predicted bump or excess luminosity versus the main peak luminosity for the suite of double detonation models in Magee et al. (2021). We use the Magee et al. (2021) models to compute luminosities in the observer-frame *o* band for a direct comparison with SN 2022ywc. As expected, SN 2022ywc stands out as an obvious outlier.

Next, we consider the ejecta–companion interaction scenario wherein SN ejecta colliding with a nondegenerate companion in the SD regime is shock-heated and drives a blue, UV-bright early excess (Kasen 2010). The detection of an early excess in this scenario is sensitive to line-of-sight effects and is predicted to be observable only in $\sim 10\%$ of the events (Kasen 2010). Apart from the viewing angle, the detection of the early excess also depends on companion mass, binary separation, and survey cadence, and sensitivity (Wang et al. 2021). Although the fraction of events with a detectable early excess in this

scenario may be higher than originally suggested, it nonetheless has a strong viewing angle dependence. The propensity for an early excess in Ia-02es suggests this feature may well be ubiquitous, and thus makes the ejecta–companion interaction a less compelling scenario for this subclass in general. For the specific case of SN 2022ywc, we examine the scaling relations in Kasen (2010) for the luminosity from ejecta–companion interaction, $L \propto aE_{\rm k}^{7/8}M_{\rm ej}^{-7/8}$, where a is the binary separation. Using a similar line of reasoning as Cao et al. (2016), we estimate that the extraordinarily luminous early excess of SN 2022ywc in the c, o bands would require a kinetic energy $E_{\rm k} \sim 2 \times 10^{52}$ erg. This is an order of magnitude higher than the explosion energy expected from the disruption of a white dwarf (eg., Jha et al. 2019), and also incompatible with the estimated kinetic energy from our MOSFiT model of $E_{\rm k} \sim 1.3 \times 10^{51}$ erg. Given the constraints on ejecta velocity from spectra, and considering a reasonable range for WD progenitor masses, we conclude that the inferred kinetic energy for ejecta–companion interaction is too high and thus also rule out this scenario for the early excess observed in SN 2022ywc.

4.2. Implications for the Progenitor Scenario

The ubiquity of early excess features in 02es-like SNe Ia would suggest a physical mechanism that is more isotropic in nature (Burke et al. 2021), as opposed to ejecta–companion interaction. It can be challenging to make a conclusive assessment for the scenario producing the early excess, even when high-cadence multiband observations are available (Noebauer et al. 2017). The remarkably luminous early excess of SN 2022ywc allows us to rule out surface radioactivity scenarios such as ^{56}Ni clumps in the outer ejecta (Magee et al.

2020) and thick He shell detonations (Polin et al. 2019), and also ejecta–companion interaction (Kasen 2010).

Cao et al. (2015) invoked ejecta–companion interaction for the UV-bright early excess of iPTF14atg. However, only a specific optically thin CSM configuration was ruled out in that study (Kromer et al. 2016; Taubenberger 2017). Additionally, Kromer et al. (2016) had difficulty reconciling the overall properties of iPTF14atg in terms of the SD scenario required for companion interaction, and instead favored a DD scenario involving a violent merger of sub-M_{Ch} WDs (Pakmor et al. 2013). A violent merger scenario was also favored for 02es-like events SN 2002es (Ganeshalingam et al. 2012), SN 2010lp (Kromer et al. 2013), and PTF10ops (Maguire et al. 2011). The DD scenario for 02es-like events is strengthened by the detection of [O I] emission in nebular spectra of SN 2010lp (Taubenberger et al. 2013) and iPTF14atg (Kromer et al. 2016). The strong [Ca II] emission in the nebular spectra of SN 2019yvq led Siebert et al. (2020) to favor a double detonation scenario, wherein an ignition in the He shell can cause a subsequent detonation in the carbon–oxygen core of a sub-M_{Ch} WD (Fink et al. 2010; Sim et al. 2010). However, Tucker et al. (2021) note that the combination of peculiar properties of SN 2019yvq including low luminosity, high velocity, and lack of [O I] emission in nebular spectra are not easily reconciled with a single explosion model. A double detonation scenario was also invoked for SN 2016jhr by Jiang et al. (2017), where the products of He shell burning account for the early excess in the light curve and the prominent Ti II trough in the spectra. Jiang et al. (2017) suggest a model with a He shell mass of $\sim 0.05\ M_\odot$ and a primary WD mass in the range 1.28–1.38$M_\odot$, consistent with our M_{ej} estimate for SN 2022ywc.

We thus favor CSM interaction as the likely scenario to explain this feature for SN 2022ywc, and potentially for 02es-like events in general by extension. Our MOSFiT model for SN 2022ywc requires $\sim 0.05\ M_\odot$ of CSM, although its origin is unclear. A carbon–oxygen (CO) rich CSM can result in the DD scenario wherein the secondary WD is disrupted by the primary, forming a centrifugally supported disk (Yoon et al. 2007; Shen et al. 2012). Simulations of WD mergers indicate that disruption of the secondary can eject $\sim 10^{-4}$–$10^{-2} M_\odot$ of material in the form of tidal tails (Raskin & Kasen 2013; Dan et al. 2014). The CSM distance in this case would depend on the time lag between the ejection of the tidal tails and eventual explosion of the merged system. The simulations by Raskin & Kasen (2013) suggest CSM distances of $\sim 10^{13}$–10^{14} cm for a time lag of $\sim 10^6$ s (~ 10 days). This scenario involving a white dwarf exploding within a $\sim 10^{-2}$–$10^{-1} M_\odot$ CO-rich envelope has also been favored recently for 03fg-like SNe Ia (eg., Ashall et al. 2021; Maeda et al. 2023). Another possibility is the CSM originating in the SD scenario involving a WD + He star binary (Neunteufel et al. 2016).

Alternatively, the accretion disk formed following the disruption of the secondary WD could launch wind-driven material during the viscous phase of the merger along the polar directions, termed disk-originated matter (DOM; Levanon et al. 2015; Levanon & Soker 2017). This model predicts $\sim 10^{-2}$–$10^{-1} M_\odot$ of DOM driven at ~ 5000 km s^{-1} (Levanon & Soker 2019). If the explosion occurs within a few hours to days of the merger, the ejecta–DOM interaction would produce a detectable early excess. Assuming $v_{DOM} \sim 5000$ km s^{-1} and $v_{ejecta} \sim 13{,}000$ km s^{-1} (from the MOSFiT model), the

estimated time lag between merger and explosion is ~ 3 days. The nonspherical configuration of the DOM could imply a favorable viewing angle along the polar axis for a small fraction of 02es-like events that would exhibit a pronounced early excess like SN 2022ywc. Although this scenario presents a unified picture that is appealing, a larger sample and detailed modeling will be required to ascertain if it can reproduce the range of luminosity, colors, and timescales for the early excess observed in 02es-like SNe Ia.

The overall photometric and spectroscopic properties of SN 2022ywc (except for the luminous early excess) such as peak luminosity and decline rate (Figure 1), and the prominent Ti II trough in the spectra (Figure 4) establish a connection with 02es-like SNe Ia in general, and in particular with hybrid 02es-like events such as SN 2006bt (Foley et al. 2010), SN 2007cq (Ganeshalingam et al. 2010), and SN 2016jhr (Jiang et al. 2017). The CSM or DOM interaction scenario would require the secondary WD to be completely disrupted and accreted during the merger process (Levanon & Soker 2019). This would disfavor a classic double detonation scenario for SN 2022ywc since the secondary WD is expected to be intact when the primary explodes and is assumed to survive (Pakmor et al. 2013), although recent simulations by Pakmor et al. (2022) investigate an interesting scenario where the secondary WD also explodes.

The evidence for He ash in the spectra of SN 2022ywc could be plausibly explained by a merger involving a primary CO WD and a secondary He or HeCO WD (Tucker et al. 2021); however, detailed numerical simulations will be needed to confront this model with observations.

4.3. Ia-02es and Ia-03fg: Closely Connected?

Although disparate in terms of their peak luminosity, we note that 03fg-like and 02es-like SNe Ia share some traits that might suggest a common origin. Similar to 02es-like SNe Ia, recent 03fg-like events discovered at early times also display an early excess feature that has been attributed to ejecta–CSM interaction (Jiang et al. 2021; Dimitriadis et al. 2023; Srivastav et al. 2023), suggesting this could be a unifying characteristic. Other similarities include weak or absent secondary i-band maxima (Ashall et al. 2021; Burke et al. 2021), ejecta velocities that are typically lower than normal SNe Ia (although there are exceptions), and detection of [O I] emission in nebular spectra in some members of both subclasses (Taubenberger et al. 2013; Kromer et al. 2016; Taubenberger et al. 2019; Dimitriadis et al. 2023). Early and late-time observations of a statistically large sample of 02es- and 03fg-like SNe Ia in the local volume will enable an in-depth investigation into this plausible connection.

5. Conclusions

We have presented observations and analysis of the hybrid 02es-like Ia SN 2022ywc, which shows a striking early excess in its light curve with no precedent in the literature. The remarkable luminosity of the early excess enables us to rule out surface radioactivity and ejecta–companion interaction scenarios. CSM interaction is favored as the likely scenario to power the early excess for SN 2022ywc, and potentially for the subclass of Ia-02es in general. Our MOSFiT model indicates a CSM mass of $\sim 0.05\ M_\odot$ at a distance of $\sim 3 \times 10^{14}$ cm from the WD. The origin of the CSM may be explained by ejection of tidal tails during a WD merger (Raskin & Kasen 2013), or

DOM launched in bipolar directions from the accretion disk following the disruption of the secondary WD (Levanon & Soker 2019). An asymmetric CSM configuration may be realized in either scenario.

The lack of multiwavelength photometric observations (eg., UV and radio) for SN 2022ywc and concurrent spectroscopic observations during the early excess limits us from placing stringent constraints on the CSM properties. Synchrotron radiation from relativistic electrons produced from ejecta–CSM interaction is expected to give rise to a luminous excess in the high frequency radio regime ($\sim$250 GHz), which could last for a few days past explosion (Hu et al. 2023). A multiwavelength observational campaign will thus be imperative for the next SN 2022ywc-like event to better understand the nature of these explosions. Nebular phase observations for SN 2022ywc (and in general for Ia-02es and Ia-03fg) would also be important for further constraining the nature of the progenitor (eg., Siebert et al. 2023).

Acknowledgments

Data Availability

Photometric data of SN 2022ywc are publicly available through the ATLAS forced photometry server (Shingles et al. 2021). The stacked ATLAS photometry presented in Figure 1 is available in the online version in machine-readable form. Spectroscopic data of SN 2022ywc are available on the Weizmann Interactive Supernova Data Repository (Yaron & Gal-Yam 2012).

ORCID iDs

Shubham Srivastav ⓘ https://orcid.org/0000-0003-4524-6883
T. Moore ⓘ https://orcid.org/0000-0001-8385-3727
M. Nicholl ⓘ https://orcid.org/0000-0002-2555-3192
M. R. Magee ⓘ https://orcid.org/0000-0002-0629-8931
S. J. Smartt ⓘ https://orcid.org/0000-0002-8229-1731
M. D. Fulton ⓘ https://orcid.org/0000-0003-1916-0664
S. A. Sim ⓘ https://orcid.org/0000-0002-9774-1192
J. M. Pollin ⓘ https://orcid.org/0009-0005-6989-3198
L. Galbany ⓘ https://orcid.org/0000-0002-1296-6887
C. Inserra ⓘ https://orcid.org/0000-0002-3968-4409
A. Kozyreva ⓘ https://orcid.org/0000-0001-9598-8821
Takashi J. Moriya ⓘ https://orcid.org/0000-0003-1169-1954
F. P. Callan ⓘ https://orcid.org/0000-0002-7975-8185
X. Sheng ⓘ https://orcid.org/0000-0002-6527-1368
K. W. Smith ⓘ https://orcid.org/0000-0001-9535-3199
J. S. Sommer ⓘ https://orcid.org/0000-0002-1154-8317
J. P. Anderson ⓘ https://orcid.org/0000-0003-0227-3451
M. Deckers ⓘ https://orcid.org/0000-0001-8857-9843
M. Gromadzki ⓘ https://orcid.org/0000-0002-1650-1518
T. E. Müller-Bravo ⓘ https://orcid.org/0000-0003-3939-7167
G. Pignata ⓘ https://orcid.org/0000-0003-0006-0188
A. Rest ⓘ https://orcid.org/0000-0002-4410-5387
D. R. Young ⓘ https://orcid.org/0000-0002-1229-2499

References

Arnett, W. D. 1982, ApJ, 253, 785
Ashall, C., Lu, J., Hsiao, E. Y., et al. 2021, ApJ, 922, 205
Astropy Collaboration, Price-Whelan, A. M., Sipőcz, B. M., et al. 2018, AJ, 156, 123
Astropy Collaboration, Robitaille, T. P., Tollerud, E. J., et al. 2013, A&A, 558, A33
Burke, J., Howell, D. A., Sarbadhicary, S. K., et al. 2021, ApJ, 919, 142
Cao, Y., Kulkarni, S. R., Gal-Yam, A., et al. 2016, ApJ, 832, 86
Cao, Y., Kulkarni, S. R., Howell, D. A., et al. 2015, Natur, 521, 328
Cappellaro, E., Mazzali, P. A., Benetti, S., et al. 1997, A&A, 328, 203
Chatzopoulos, E., Wheeler, J. C., & Vinko, J. 2012, ApJ, 746, 121
Chatzopoulos, E., Wheeler, J. C., Vinko, J., Horvath, Z. L., & Nagy, A. 2013, ApJ, 773, 76
Chevalier, R. A., & Irwin, C. M. 2011, ApJL, 729, L6
Collins, C. E., Gronow, S., Sim, S. A., & Röpke, F. K. 2022, MNRAS, 517, 5289
Collins, C. E., Sim, S. A., Shingles, L. J., et al. 2023, MNRAS, 524, 4447
Dan, M., Rosswog, S., Brüggen, M., & Podsiadlowski, P. 2014, MNRAS, 438, 14
De, K., Kasliwal, M. M., Polin, A., et al. 2019, ApJL, 873, L18
Deckers, M., Maguire, K., Magee, M. R., et al. 2022, MNRAS, 512, 1317
Dimitriadis, G., Foley, R. J., Rest, A., et al. 2019, ApJL, 870, L1
Dimitriadis, G., Maguire, K., Karambelkar, V. R., et al. 2023, MNRAS, 521, 1162
Dong, Y., Valenti, S., Polin, A., et al. 2022, ApJ, 934, 102
Fink, M., Röpke, F. K., Hillebrandt, W., et al. 2010, A&A, 514, A53
Foley, R. J., Narayan, G., Challis, P. J., et al. 2010, ApJ, 708, 1748
Ganeshalingam, M., Li, W., Filippenko, A. V., et al. 2010, ApJS, 190, 418
Ganeshalingam, M., Li, W., Filippenko, A. V., et al. 2012, ApJ, 751, 142
Guillochon, J., Nicholl, M., Villar, V. A., et al. 2018, ApJS, 236, 6
Hachinger, S., Mazzali, P. A., Taubenberger, S., et al. 2012, MNRAS, 422, 70

Hosseinzadeh, G., Sand, D. J., Sarbadhicary, S. K., et al. 2023, ApJL, 953, L15
Hosseinzadeh, G., Sand, D. J., Valenti, S., et al. 2017, ApJL, 845, L11
Hu, M., Wang, L., Wang, X., & Wang, L. 2023, MNRAS, 525, 246
Ihanec, N., Kravtsov, T., Gromadzki, M., Grzesiak, K., & Bruch, R. J. 2022, TNSCR, 2022-3336, 1
Jha, S. W., Maguire, K., & Sullivan, M. 2019, NatAs, 3, 706
Jiang, J.-A., Doi, M., Maeda, K., et al. 2017, Natur, 550, 80
Jiang, J.-A., Doi, M., Maeda, K., & Shigeyama, T. 2018, ApJ, 865, 149
Jiang, J.-a., Maeda, K., Kawabata, M., et al. 2021, ApJL, 923, L8
Jones, D. H., Read, M. A., Saunders, W., et al. 2009, MNRAS, 399, 683
Kasen, D. 2010, ApJ, 708, 1025
Kromer, M., Fremling, C., Pakmor, R., et al. 2016, MNRAS, 459, 4428
Kromer, M., Pakmor, R., Taubenberger, S., et al. 2013, ApJL, 778, L18
Kromer, M., Sim, S. A., Fink, M., et al. 2010, ApJ, 719, 1067
Levanon, N., & Soker, N. 2017, MNRAS, 470, 2510
Levanon, N., & Soker, N. 2019, ApJL, 872, L7
Levanon, N., Soker, N., & García-Berro, E. 2015, MNRAS, 447, 2803
Li, W., Wang, X., Vinkó, J., et al. 2019, ApJ, 870, 12
Liu, C., Miller, A. A., Polin, A., et al. 2023a, ApJ, 946, 83
Liu, Z.-W., Roepke, F. K., & Han, Z. 2023b, RAA, 23, 082001
Livio, M., & Mazzali, P. 2018, PhR, 736, 1
Maeda, K., Jiang, J.-A., Doi, M., Kawabata, M., & Shigeyama, T. 2023, MNRAS, 521, 1897
Maeda, K., Jiang, J.-A., Shigeyama, T., & Doi, M. 2018, ApJ, 861, 78
Magee, M. R., Cuddy, C., Maguire, K., et al. 2022, MNRAS, 513, 3035
Magee, M. R., Maguire, K., Kotak, R., et al. 2020, A&A, 634, A37
Magee, M. R., Maguire, K., Kotak, R., & Sim, S. A. 2021, MNRAS, 502, 3533
Maguire, K., Sullivan, M., Thomas, R. C., et al. 2011, MNRAS, 418, 747
Matheson, T., Kirshner, R. P., Challis, P., et al. 2008, AJ, 135, 1598
Mazzali, P. A., Sullivan, M., Hachinger, S., et al. 2014, MNRAS, 439, 1959
Miller, A. A., Magee, M. R., Polin, A., et al. 2020, ApJ, 898, 56
Moriya, T. J., Mazzali, P. A., Ashall, C., & Pian, E. 2023, MNRAS, 522, 6035
Nadyozhin, D. K. 1994, ApJS, 92, 527
Neunteufel, P., Yoon, S. C., & Langer, N. 2016, A&A, 589, A43
Nicholl, M., Guillochon, J., & Berger, E. 2017, ApJ, 850, 55
Noebauer, U. M., Kromer, M., Taubenberger, S., et al. 2017, MNRAS, 472, 2787

Pakmor, R., Callan, F. P., Collins, C. E., et al. 2022, MNRAS, 517, 5260
Pakmor, R., Kromer, M., Taubenberger, S., & Springel, V. 2013, ApJL, 770, L8
Piro, A. L., Haynie, A., & Yao, Y. 2021, ApJ, 909, 209
Piro, A. L., & Morozova, V. S. 2016, ApJ, 826, 96
Polin, A., Nugent, P., & Kasen, D. 2019, ApJ, 873, 84
Predehl, P., & Schmitt, J. H. M. M. 1995, A&A, 293, 889
Raskin, C., & Kasen, D. 2013, ApJ, 772, 1
Schlafly, E. F., & Finkbeiner, D. P. 2011, ApJ, 737, 103
Shappee, B. J., Holoien, T. W. S., Drout, M. R., et al. 2019, ApJ, 870, 13
Shen, K. J., Bildsten, L., Kasen, D., & Quataert, E. 2012, ApJ, 748, 35
Shingles, L., Smith, K. W., Young, D. R., et al. 2021, TNSAN, 7, 1
Siebert, M. R., Dimitriadis, G., Polin, A., & Foley, R. J. 2020, ApJL, 900, L27
Siebert, M. R., Foley, R. J., Zenati, Y., et al. 2023, arXiv:2306.11788
Silverman, J. M., Foley, R. J., Filippenko, A. V., et al. 2012, MNRAS, 425, 1789
Sim, S. A., Röpke, F. K., Hillebrandt, W., et al. 2010, ApJL, 714, L52
Smartt, S. J., Valenti, S., Fraser, M., et al. 2015, A&A, 579, A40
Smith, K. W., Smartt, S. J., Young, D. R., et al. 2020, PASP, 132, 085002
Snodgrass, C., Saviane, I., Monaco, L., & Sinclaire, P. 2008, Msngr, 132, 18
Speagle, J. S. 2020, MNRAS, 493, 3132
Srivastav, S., Smartt, S. J., Huber, M. E., et al. 2023, ApJL, 943, L20
Taubenberger, S. 2017, in The Extremes of Thermonuclear Supernovae, Handbook of Supernovae, ed. A. W. Alsabti & P. Murdin (Berlin: Springer), 317
Taubenberger, S., Floers, A., Vogl, C., et al. 2019, MNRAS, 488, 5473
Taubenberger, S., Kromer, M., Pakmor, R., et al. 2013, ApJL, 775, L43
Tonry, J., Denneau, L., Weiland, H., et al. 2022, TNSTR, 2022-3139, 1
Tonry, J. L., Denneau, L., Flewelling, H., et al. 2018a, ApJ, 867, 105
Tonry, J. L., Denneau, L., Heinze, A. N., et al. 2018b, PASP, 130, 064505
Tucker, M. A., Ashall, C., Shappee, B. J., et al. 2021, ApJ, 914, 50
Wang, Q., Rest, A., Dimitriadis, G., et al. 2023, arXiv:2305.03779
Wang, Q., Rest, A., Zenati, Y., et al. 2021, ApJ, 923, 167
White, C. J., Kasliwal, M. M., Nugent, P. E., et al. 2015, ApJ, 799, 52
Yaron, O., & Gal-Yam, A. 2012, PASP, 124, 668
Yoon, S. C., Podsiadlowski, P., & Rosswog, S. 2007, MNRAS, 380, 933
Zhang, K., Wang, X., Zhang, J., et al. 2016, ApJ, 820, 67